Proceedings of the 17th World Congress
The International Federation of Automatic Control
Seoul, Korea, July 6-11, 2008

Direct Torque Tracking PI-Controller Design for Switched Reluctance Motor Drive using Singular Perturbation Method

Sanjib Kumar Sahoo * **Sanjib Kumar Panda** ** **Jian-Xin Xu** ***
Valery D. Yurkevich ****

* *Department of Electrical and Computer Engineering, National University of Singapore, 4 Engineering Drive-3, Singapore, 117576; (e-mail: elesahoo@nus.edu.sg)*
** *Department of Electrical and Computer Engineering, National University of Singapore, 4 Engineering Drive-3, Singapore, 117576; (e-mail: eleskp@nus.edu.sg)*
*** *Department of Electrical and Computer Engineering, National University of Singapore, 4 Engineering Drive-3, Singapore, 117576; (e-mail: elejxx@nus.edu.sg)*
**** *Automation Department of Novosibirsk State Technical University, Novosibirsk, 630092, Russia.(e-mail: yurkev@ac.cs.nstu.ru)*

Abstract: The problem of torque tracking PI-controller design for switched reluctance motor (SRM) drive is discussed, where SRM magnetization characteristics are highly nonlinear, and torque is a complex and coupled function of phase current and rotor position. A distinctive feature of the control system designed is that two-time-scale motions are artificially forced in the closed-loop system by the selection of control law parameters. Hence, singular perturbation method is used to analyze the closed-loop system properties. Stability conditions imposed on the fast and slow modes, and a sufficiently large mode separation rate, can ensure that after fast ending of the fast-motion transients, the torque tracking error dynamics are as desired by the control system design specifications and they are insensitive to SRM nonlinearities. An accurate polynomial model of a prototype SRM magnetization characteristics is used for simulation studies of the proposed controller. However, only a simple trapezoidal profile for SRM inductance is used for calculation of the control voltage. Simulation results for constant motor torque at different speeds show that motor peak-to-peak torque ripples are minimized to about 5% of the average torque, especially for low speed operation.

Keywords: switched reluctance motor, direct torque control, robust tracking control, singular perturbation method

1. INTRODUCTION

SRM has a robust mechanical structure and many advantages over other electromagnetic motors. These include: windings only on stator poles facilitate ease of cooling, absence of permanent magnets or winding on rotor makes it suitable for high speed operation, no shoot-through fault in power converter adds to over all drive system robustness. However, excessive torque ripples due to the difficulty in torque control has made it unpopular for high-performance drive applications. Torque ripples are particularly critical at low speed operation when these may cause speed ripples and lead to degradation in the product quality.

Many researchers have proposed SRM torque controllers similar to other drives as shown by Husain [2002], by converting torque reference into current reference and then using current controllers to realize the currents in the phase windings. However, due to the highly nonlinear and complex nature of SRM magnetization characteristics, torque-to-current conversion becomes quite complex and prone to error.

Alternatively, direct torque control (DTC) scheme does not need to convert the torque reference to equivalent current reference. The defining characteristics of DTC are: 1) no need for torque-to-current conversion to obtain phase current reference for a given motor torque, and 2) no need for current controllers. Instead, the motor torque is estimated and compared with the reference torque, and the torque error is used for obtaining the control voltage directly.

2. NONLINEAR STATE EQUATIONS FOR DTC SCHEME

In DTC scheme, phase torque is the plant output whereas phase voltage v is the control input. Motor torque $T(i,\theta)$ being a function of both phase current i and rotor position θ, torque dynamics can be written as:

$$\frac{dT}{dt} = \left(\frac{\partial T}{\partial i}\right)\left(\frac{\partial \psi}{\partial i}\right)^{-1}\left(-iR - \frac{\partial \psi}{\partial \theta}\frac{d\theta}{dt}\right) + \frac{\partial T}{\partial \theta}\frac{d\theta}{dt} + \left(\frac{\partial T}{\partial i}\right)\left(\frac{\partial \psi}{\partial i}\right)^{-1} v. \quad (1)$$

Rewriting(1) in the form of general nonlinear state equation:

$$\dot{T} = f + bu, \quad (2)$$

where

$$f = \frac{\partial T}{\partial i}\left(\frac{\partial \psi}{\partial i}\right)^{-1}\left(-iR - \frac{\partial \psi}{\partial \theta}\frac{d\theta}{dt}\right) + \frac{\partial T}{\partial \theta}\frac{d\theta}{dt},$$
$$b = \frac{\partial T}{\partial i}\left(\frac{\partial \psi}{\partial i}\right)^{-1},$$
$$u = v. \quad (3)$$

The phase flux-linkage $\psi(i,\theta)$ is a nonlinear function as SRM is commonly operated in deep magnetic saturation. It can be seen from preceding equations that the toque dynamics are highly nonlinear and time-varying. Linear control design methods would not be able to provide high-performance.

A hysteresis type DTC for SRM had been reported by Inderka et al. [2002]. Hysteresis controller applies full DC link voltage to the phase winding and hence requires very high sampling frequency to keep the output torque within a narrow band of the reference. Any digital controller implementation requires an anti-aliasing filter, which is basically a low pass filter. This filter adds a phase lag to the feedback signal, and hence the change in current may not show in the feedback immediately. Due to this reason, a bang-bang type controller will give rise to an oscillatory output.

Instead of applying either $-V_{dc}$, $+V_{dc}$ or zero only, the controller should apply a variable voltage between $-V_{dc}$ and $+V_{dc}$ to track the torque reference smoothly, as shown by Neuhaus et al. [2006]. A pulse-width-modulated (PWM) converter is used to supply the variable voltage to the SRM. Neuhaus et al. [2006] have proposed to use flux-linkage as the control variable and use predictive, dead-beat control to achieve instantaneous torque control. However, conversion of phase torque to phase flux-linkage using a look-up table is not a direct torque control scheme as such. Secondly, estimation of flux-linkage from phase voltage integrating the volt-seconds is prone to error. Model-based nonlinear control technique such as feedback linearization used by Panda et al. [1996] requires an accurate plant model. As modelling of SRM magnetization characteristics is difficult and prone to error due to manufacturing tolerances, the controller should be robust to model inaccuracies.

A control design method has been proposed in this paper where two-time-scale motions are artificially forced in the closed-loop system by proper selection of control law parameters. Hence, control system properties are analyzed using singular perturbation method. A PI controller results from this method which is implemented using a digital controller. The following sections show the proposed torque controller structure, design methodology and simulation results.

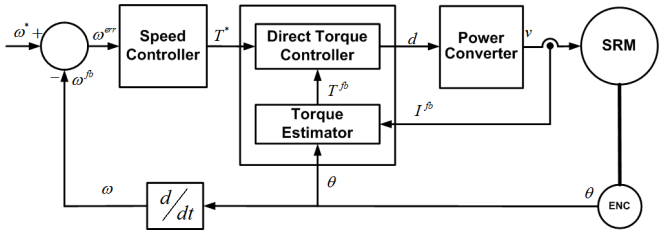

Fig. 1. Block diagram of speed control system using an SRM: ω^*-speed reference; ω^{fb}-speed feedback; T^* is the motor torque reference, T^{fb} is motor torque feedback from the torque estimator, d is duty cycle from torque controller, v phase winding voltages from the converter, θ is position feedback from the encoder

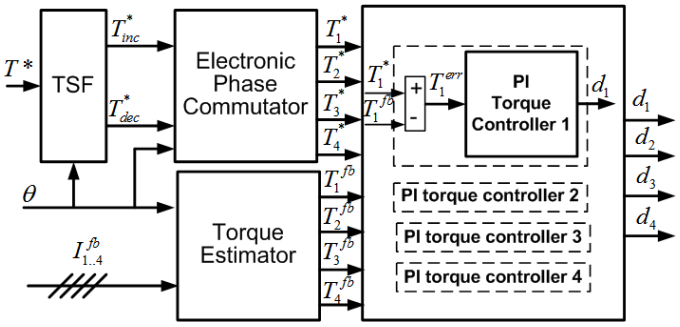

Fig. 2. Four PI torque controllers for the four phase windings

Table 1. Specifications of Prototype SRM

Rated Power	$1\,hp$
No. of poles	8/6
Max speed	$4000\,rmin$
Rated Torque	$1.78\,N.m$

3. SRM BASED MOTION CONTROL SYSTEM

The block diagram of a speed control system using switched reluctance motors is shown in Fig.1. The speed controller generates the motor torque reference T^* for the torque controller. Fig.2 shows the internal details of the torque controller for SRM.

Due to limited available DC-link voltage and finite phase winding inductance; the phase currents, and therefore phase torques can not be commutated instantaneously. First, a torque sharing function (TSF) distributes the motor torque among the phase windings so that phase torque references do not change instantaneously. For the laboratory prototype SRM given in Table 1, Fig.3 shows the TSF that distributes the demanded torque T^* among two neighboring phases, T^*_{inc} and T^*_{dec}; thereby ensuring a smooth and trackable growth and fall of the torque demand for each phase. The phase just entering into the torque producing region has to produce T^*_{inc} whereas the phase nearing the aligned position has to produce T^*_{dec}. As infinitely many TSFs can satisfy this requirement; additional constraints like efficiency and operating speed range should be considered for deciding the TSF. A TSF

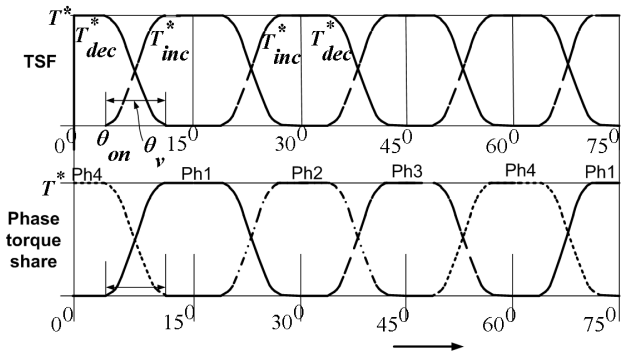

Fig. 3. Cubic torque sharing function with the phase torque shares; θ_{on} is the starting point of the overlap region; θ_v the width of the overlapping region when two nearby phases actually share the total motor torque

with a cubic segment as defined in (5)-(6) has been used in this work as cubic polynomials are the simplest functions to provide smooth phase torque references.

$$\begin{aligned} T^*_{inc} &= f(\theta) \\ T^*_{dec} &= T^* - T^*_{inc}. \end{aligned} \tag{4}$$

$$f(\theta) = A + B(\theta - \theta_{on}) + C(\theta - \theta_{on})^2 + D(\theta - \theta_{on})^3 \tag{5}$$

where,

$$A = 0\,;\; B = 0\,;\; C = \frac{3T^*}{\theta_v^2}\,;\; D = -\frac{2T^*}{\theta_v^3}\,, \tag{6}$$

with θ_{on} is the starting point for phase current conduction and θ_v is the width of the overlapping region of conduction between two neighboring phases.

The next task is to realize the phase torque references by applying suitable control techniques. An accurate closed-loop torque controller needs the actual motor torque as feedback. The phase currents and rotor position are given as feedback to the torque estimator for estimation of motor torque. The following section discusses the torque estimator used for torque feedback.

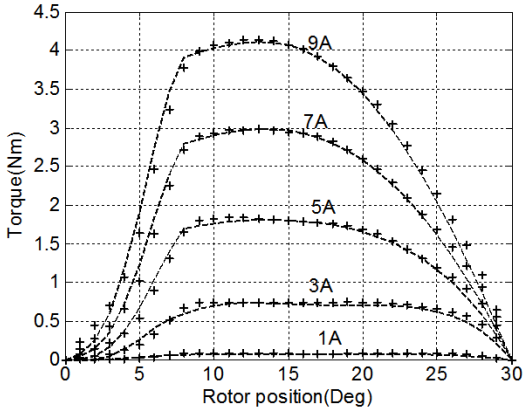

Fig. 4. Matching of measured static torque data (–) with the torque predicted by the torque estimator(+) derived from the polynomial flux-linkage model.

3.1 Torque feedback

Commonly, a strain-gauge type of torque transducer is used for measurement of torque. However, this is bulky, expensive and needs space for installation. An accurate torque estimator in terms of phase current and rotor position is developed from a flux-linkage model $\psi(i,\theta)$. First, the flux-linkage had been measured at different rotor position from $0^0 - 30^0$ and phase current values from $1\,A - 9\,A$. This range of rotor position and phase current were divided into four regions: 1) for small currents near unaligned position, 2) for small currents near aligned position, 3) for large currents near unaligned rotor position and, 4) for large currents near aligned position. Fifth order polynomials are used for capturing the variation of flux-linkage with rotor position with current being constant. Then, variation of the polynomial coefficients for different currents is again captured by another fifth order polynomial in current. Finally, the torque estimator is derived from flux-linkage model using co-energy principle i.e. $T(i,\theta) = \frac{\partial}{\partial\theta}\int_0^i \psi(\iota,\theta)d\iota$. The torque estimator is given as:

$$\begin{aligned} T(i,\theta) &= \sum_{k=1}^{5}\left(\sum_{m=0}^{5} N_{1,k,1,m}\frac{i^{m+1}}{m+1}\right)k\theta^{k-1} \\ &\quad (\text{for } 0 \le i \le i_s \text{ and } 0 \le \theta \le \theta_h) \\ &= \sum_{k=1}^{5}\left(\sum_{m=0}^{5} N_{2,k,1,m}\frac{i^{m+1}}{m+1}\right)k\theta^{k-1} \\ &\quad (\text{ for } 0 \le i \le i_s \text{ and } \theta_h \le \theta \le \theta_a) \\ &= T_1(i_s,\theta) + \\ &\quad \sum_{k=1}^{5}\left(\sum_{m=0}^{5} N_{1,k,2,m}\frac{i^{m+1} - i_s^{m+1}}{m+1}\right)k\theta^{k-1} \\ &\quad (\text{for } i_s \le i \le i_{max} \text{ and } 0 \le \theta \le \theta_h \\ &= T_2(i_s,\theta) + \\ &\quad \sum_{k=1}^{5}\left(\sum_{m=0}^{5} N_{2,k,2,m}\frac{i^{m+1} - i_s^{m+1}}{m+1}\right)k\theta^{k-1} \\ &\quad (\text{for } i_s \le i \le i_{max} \text{ and } \theta_h \le \theta \le \theta_a, \end{aligned}$$

where

$$\begin{aligned} T_1(i_s,\theta) &= \sum_{k=1}^{5}\left(\sum_{m=0}^{5} N_{1,k,1,m}\frac{i_s^{m+1}}{m+1}\right)k\theta^{k-1}, \\ T_2(i_s,\theta) &= \sum_{k=1}^{5}\left(\sum_{m=0}^{5} N_{2,k,1,m}\frac{i_s^{m+1}}{m+1}\right)k\theta^{k-1}. \end{aligned} \tag{7}$$

The estimator was verified by comparing with the phase torque measured under locked rotor condition. As can be seen in Fig.4, the matching between the estimated torque and the measured torque is quite accurate. Hence, this torque estimator has been used for accurate torque feedback. However, the proposed two-time scale DTC scheme can be used for any other method of torque feedback as well.

4. TORQUE TRACKING PI-CONTROLLER DESIGN

4.1 Continuous-time PI-Controller

Let the tracking error be defined as $e = T^{ref} - T$, where the torque behavior is governed by (2), and the torque dynamics is given by (1). The controller is being designed so that the desired tracking error behavior given by

$$\dot{e} = -\lambda e \tag{8}$$

holds, where $\lambda > 0$.

In accordance with the design methodology Yurkevich [2004], let us consider the torque tracking error controller given by

$$\mu\dot{u} = k[\lambda e + \dot{e}], \tag{9}$$

where μ is a small positive parameter, k is a gain selected in accordance with the induced fast-motions stability requirement as shown below. Note that the control law (9) may be expressed in terms of transfer functions, of a conventional PI-controller

$$u(s) = \left[\frac{k\lambda}{\mu s} + \frac{k}{\mu}\right] e(s).$$

4.2 Two-time-scale motion analysis

In accordance with (2) and (9), consider the equations of the closed-loop system given by

$$\dot{e} = \dot{T}^{ref} - f - bu, \tag{10a}$$
$$\mu\dot{u} = k[\lambda e + \dot{e}]. \tag{10b}$$

By substituting of (10a) into (10b), the system (10) can be rewritten as

$$\dot{e} = \dot{T}^{ref} - f - bu, \tag{11a}$$
$$\mu\dot{u} = k[\lambda e + \dot{T}^{ref} - f - bu]. \tag{11b}$$

Since μ is the small positive parameter, the closed-loop system equations (11) has the standard singular perturbation form and, accordingly, the singular perturbation method (see Tikhonov [1952], Kokotović et al. [1999], Naidu [2002]) may be used to analyze the closed-loop system properties. Hence, from (11), we obtain the fast-motion subsystem (FMS) given by

$$\mu\dot{u} = -kbu + k[\lambda e + \dot{T}^{ref} - f], \tag{12}$$

where e, f, b and $\dot{T}^{ref}$ are treated as the frozen variables during the transients in (12) (that assumption can be provided by $\mu \to 0$, that leads to increase of time-scale separation degree between fast and slow modes in the closed-loop system).

Let the gain k is selected such that $kb > 0$, then the FMS is stable. Hence, after the rapid decay of transients in (12), we have the steady state (more precisely, quasi-steady state) for the FMS (12) , where $u(t) = u^s(t)$ and

$$u^s = u^{id} = b^{-1}[\lambda e + \dot{T}^{ref} - f], \tag{13}$$

where u^{id} is the nonlinear inverse dynamics solution. Substitution of (13) into (10a) yields the slow-motion subsystem (SMS) equations in the form (8). Hence, after the damping of fast transients, the desired tracking error behavior is fulfilled despite that f and g are unknown complex and coupled functions of phase current and rotor position.

The control law parameters T_s, μ, k, and λ should be selected such that it would provide: first, the FMS stability; second, the desired degree of time-scale separation between fast and slow motions in the closed-loop system (11). Note that the degree of time-scale separation η can be estimated by the ratio of SMS time constant to the FMS time constant, that is $\eta = kb/(\lambda\mu)$.

4.3 Digital PI-Controller

For implementation of the torque tracking error controller, let us consider a $\mathcal{Z}$-transform of (9) preceded by a ZOH. Hence, the pulse-transfer function of the digital PI-controller

$$H_{u/e}(z) = \frac{k}{\mu}\left[1 + \frac{\lambda T_s}{z-1}\right]$$

follows, where T_s is a sampling period.

Note that for small T_s the ZOH can be approximated by a time delay $\tau = T_s/2$ (see Åström and B. Wittenmark [1997]), then in order to consider the effect of controller discretization on the closed-loop system properties, instead of (10), a nonlinear pseudo-continuous-time model

$$\dot{e}(t) = \dot{T}^{ref}(t) - f(t) - b(t)u(t-\tau), \tag{14a}$$
$$\mu\dot{u}(t) = k[\lambda e(t) + \dot{e}(t)]. \tag{14b}$$

with the delay $\tau = T_s/2$ taken into account (see Yurkevich [2004], Yurkevich et al. [1997]). Then, from (14), we obtain the FMS given by

$$\mu\dot{u}(t) = -kb(t)u(t-\tau) + k[\lambda e(t) + \dot{T}^{ref}(t) - f(t)], \tag{15}$$

where $e(t)$, $f(t)$, $b(t)$ and $\dot{T}^{ref}(t)$ are treated as the constant values during the transients in (15).

From (15), the corresponding transfer function of the open-loop FMS with pure time delay

$$G^o_{FMS}(s) = \frac{kb\exp(-T_s s/2)}{\mu s}, \tag{16}$$

results. Then the crossover frequency ω_c and the phase margin PM on the Nyquist plot of (16) are given by $\omega_c = kb/\mu$ and $PM = [\pi - \omega_c T_s]/2$, accordingly. It is clear to see, an increase of b leads to decrease of PM given that the sampling period T_s is fixed. Hence, in order to maintain the constant value of the fast-motion subsystem phase margin PM, take $k = \hat{b}^{-1}$, where $\hat{b}$ is an estimate of the parameter b.

Assume that the sampling period T_s is fixed and $T_s = 2 \cdot 10^{-4}$ s. Take, for example, the desired phase margin PM_d given by $PM_d = 1$ rad, and the desired degree of time-scale separation given by $\eta_d = 60$. Then, from the above, the parameters μ and λ

$$\mu = \frac{T_s}{2(\pi/2 - PM_d)} \approx 1.75 \cdot 10^{-4}\, s, \quad \lambda = \frac{1}{\eta_d \mu} \approx 95\, s^{-1} \tag{17}$$

result given that the condition $kb = 1$ holds.

Value of $\hat{b}$ is obtained using a trapezoidal profile for phase inductance i.e. assuming that inductance is directly proportional to the overlap between stator and rotor poles. The analytical expression for the nominal model is $\psi(i,\theta) = L(\theta)i$ and $L(\theta)$ is given by

$$\begin{aligned} L(\theta) &= L_u, \text{ for } 0^0 < \theta \leq \theta_1 \\ &= L_u + K\,\theta^{'}; \theta^{'} = (\theta - \theta_1), \text{ for } \theta_1 < \theta \leq \theta_2 \\ &= L_a, \text{ for } \theta_2 < \theta \leq\ 30^0, \end{aligned} \tag{18}$$

where L_u is the phase inductance at the unaligned rotor position, $K = \frac{dL}{d\theta}$ is the slope of the assumed phase inductance variation vs. rotor position, $\theta = 0$ is the unaligned rotor position and $\theta = 30^0$ is the aligned rotor position. For the prototype motor, $L_u = 0.01\,H$, $L_a = 0.04\,H$, $\theta_1 = 7^0$, $\theta_2 = 27^0$, $K = 0.09\,Nm/A^2$. Then, using $T = \frac{1}{2}Ki^2$, $\frac{\partial\psi}{\partial i} = L_u + K\theta^{'}$ and $\frac{\partial T}{\partial i} = Ki$. Finally, $\hat{b}$ is obtained as:

$$\hat{b} = \frac{Ki}{L_u + K\theta^{'}} \tag{19}$$

The selection of controller parameters in accordance with the desired phase margin PM_d of the fast-motion subsystem (15) provides a guarantee of FMS stability on controller discretization. These control parameters are used in simulation of the controller. The simulation results and their analysis are provided in the next section.

5. SIMULATION RESULTS

The controller performance has been verified through numerical simulation using MATLAB-SIMULINK. Simulation is carried out for full motor torque of $1.8\,Nm$, at two speeds $40\,rpm$ and $240\,rpm$. Other important parameters were on-angle $\theta_{on} = 5^0$, overlap angle $\theta_v = 5^0$, sampling time $T_s = 200\,\mu s$ and DC-link voltage $V_{dc} = 200V$. The sampling time is chosen based on the typical execution time on our laboratory prototype controller.

First, a bang-bang type DTC scheme has been simulated. The hysteresis bandwidth was set at $0.1\,Nm$. Due to the limited sampling frequency, the phase torque does not stay within the hysteresis band. This results in excessive torque ripples, almost up to 50%, as can be seen in Fig.5. Next, the bang-bang type controller had been simulated with $V_{dc} = 48V$ (typical voltage for electric vehicle system) and $T_s = 50\mu s$. Fig.6 shows that torque ripples are much less at about 5 %. These two results indicate that bang-bang type controller can be used for low DC-link voltage and if the sampling time of the controller can be kept low. In SRM controller, the main computation involves that of the torque sharing function (TSF) and estimation of phase torque. The sampling time can be kept low with a faster processor, but that solution will be expensive. However, the proposed PI controller gives equivalent performance for the available DC-link voltage and for the same sampling time.

Fig.7 shows the motor torque and two phase torques with motor operating at $1.8\,Nm$ and $40\,rpm$. It can be seen that torque tracking ripples are negligible. Next, simulations are carried out for $240\,rpm$. Fig.8 shows the motor torque with two phase torques. The peak-to-peak ripples have increased to about $0.1\,Nm$, which is about 5% of the average torque. This result is very promising considering the fact that the controller design is quite simple. Fig.9 shows the torque reference and corresponding estimated torque for one phase winding. The phase torque tracking error is shown to be within $\pm 0.15\,Nm$. Corresponding phase current and phase voltages are shown in Fig.10, which show that phase current stays controlled for the proposed DTC scheme. The phase voltage is high during the increasing and decreasing part of the phase torque reference, as expected.

It can also be noted that the phase torque tracking error and motor torque ripples increase with increasing speed. This is explained by the fact that bandwidth of the controller (λ) is fixed, whereas the bandwidth of the phase torque references increases with motor speed.

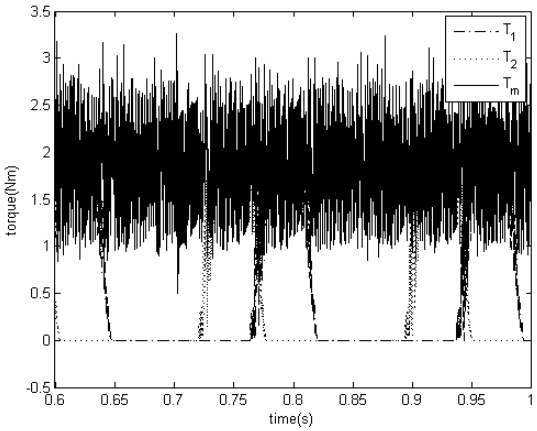

Fig. 5. Simulation results for a bang-bang type DTC scheme: actual motor torque showing the torque ripples and two phase torques, with motor speed 40 rpm, motor torque at 1.8 Nm, with $V_{dc} = 200V$ and $T_s = 200\mu s$

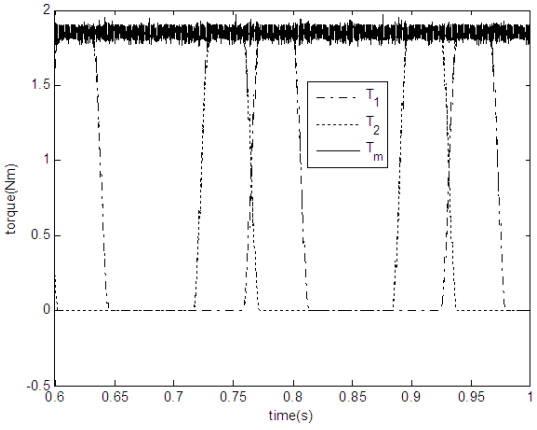

Fig. 6. Simulation results for a bang-bang type DTC scheme: actual motor torque showing the torque ripples and two phase torques, with motor speed 40 rpm, motor torque at 1.8 Nm, with $V_{dc} = 48V$ and $T_s = 50\mu s$

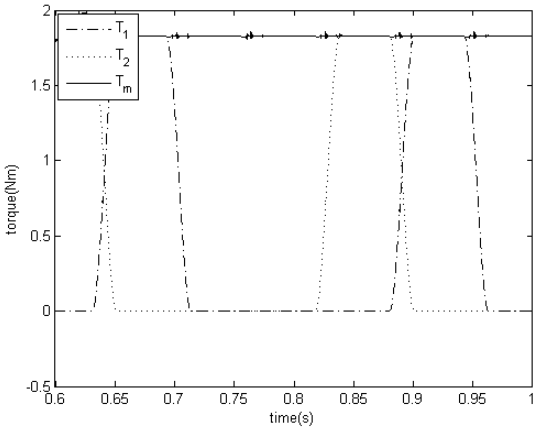

Fig. 7. Simulation results for proposed PI based DTC: actual motor torque showing the torque ripples and two phase torques, with motor speed 40 rpm, motor torque at 1.8 Nm

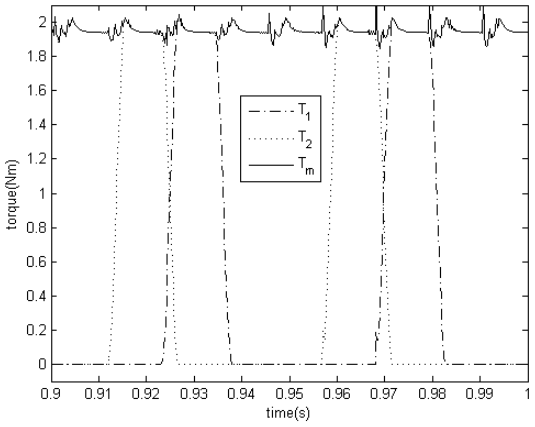

Fig. 8. Simulation results for proposed PI based DTC: actual motor torque showing the torque ripples and two phase torques, with motor speed 240 rpm, motor torque at 1.8 Nm

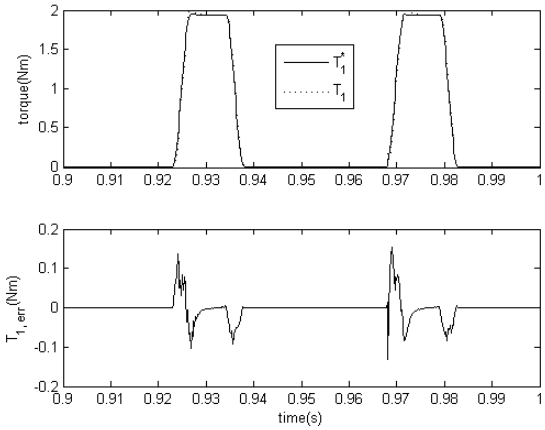

Fig. 9. Simulation results for proposed PI based DTC: phase1 torque reference, actual torque and tracking error in Nm; with motor speed 240 rpm, motor torque at 1.8 Nm

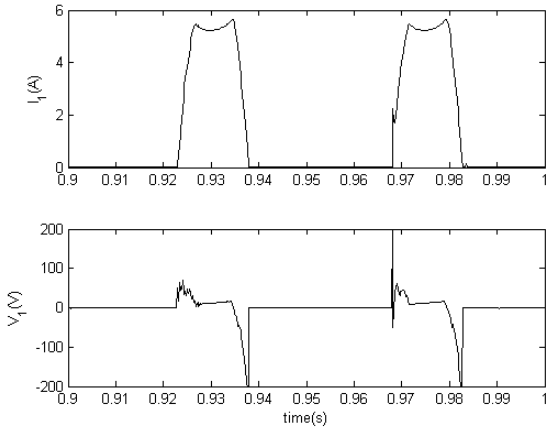

Fig. 10. Simulation results for proposed PI based DTC: phase1 current and voltage; with motor speed 240 rpm, motor torque at 1.8 Nm

REFERENCES

I. Husain. Minimization of torque ripple in SRM drives. *IEEE Trans. Ind. Electron.*, volume 49, no. 1, pages 28–39, Feb. 2002.

R. B. Inderka, and R. W. De Doncker. DITC-direct instantaneous torque control of switched reluctance drives. *IEEE IAS Annual Meeting*, volume 3, pages 1605-1609, 2002.

C. R. Neuhaus, N. H. Fuengwarodsakul, and R. W. De Doncker. Predictive PWM-based Direct Instantaneous Torque Control of Switched Reluctance Drives. *37th IEEE Power Electronics Specialists Conference,* pages 3240-3246, June, 2006, Jeju, Korea.

S. K. Panda, P. K. Dash. Application of nonlinear control to switched reluctance motors: a feedback linearisation approach. *IEE Proc., Electric Power Applications*, volume 143, no. 5, pages 371-379, Sept. 1996.

V. D. Yurkevich. Design of nonlinear control systems with the highest derivative in feedback, *Series on Stability, Vibration and Control of Systems*, Series A - volume 16, World Scientific, 2004, 352 p.

P. V. Kokotović, H. K. Khalil, and J.O'Reilly. *Singular Perturbation Methods in Control: Analysis and Design*, Philadelphia, PA: SIAM, 1999.

A.N. Tikhonov. Systems of differential equations containing a small parameter multiplying the derivative. *Mathematical Sb.*, Moscow, volume 31, no. 3, pages 575–586, 1952.

D. S. Naidu. Singular Perturbations and Time Scales in Control Theory and Applications: An Overview. *Dynamics of Continuous, Discrete & Impulsive Systems (DCDIS)* Series B: Applications & Algorithms, volume 9, no. 2, pages 233-278, June 2002.

K.J. Åström, B. Wittenmark. *Computer-controlled systems: theory and design*, 3rd ed., Prentice-Hall information and system sciences series, Upper Saddle River, N.J. : Prentice Hall, 1997, 557 p.

V. D. Yurkevich, M. J. Błachuta, and K. Wojciechowski. Design of digital controllers for MIMO non-linear time-varying systems based on dynamic contraction method. *Proc. of European Control Conf. (ECC'97)*, Brussels, Belgium, 1997.